J. Marine Sci. Appl. (2012) 11: 410-416
DOI: 10.1007/s11804-012-1150-1

Numerical Prediction of Added Resistance and Vertical Ship Motions in Regular Head Waves

Haixuan Ye, Zhirong Shen and Decheng Wan*

State Key Laboratory of Ocean Engineering, School of Naval Architecture, Ocean and Civil Engineering, Shanghai Jiao Tong University, Shanghai 200240, China

Abstract: The numerical prediction of added resistance and vertical ship motions of one ITTC (International Towing Tank Conference) S-175 containership in regular head waves by our own in-house unsteady RANS solver naoe-FOAM-SJTU is presented in this paper. The development of the solver naoe-FOAM-SJTU is based on the open source CFD tool, OpenFOAM. Numerical analysis is focused on the added resistance and vertical ship motions (heave and pitch motions) with four very different wavelengths ($0.8L_{pp} \le \lambda \le 1.5L_{pp}$) in regular head waves. Once the wavelength is near the length of the ship model, the responses of the resistance and ship motions become strongly influenced by nonlinear factors, as a result difficulties within simulations occur. In the paper, a comparison of the experimental results and the nonlinear strip theory was reviewed and based on the findings, the RANS simulations by the solver naoe-FOAM-SJTU were considered competent with the prediction of added resistance and vertical ship motions in a wide range of wave lengths.
Keywords: added resistance; vertical ship motions; S-175 ship model; naoe-FOAM-SJTU solver; regular waves
Article ID: 1671-9433(2012)04-0410-07

1 Introduction

The increase of the resistance due to waves encountered in comparison with calm water resistance under the condition of same ship speed is called added resistance and is a very important study in ship designs. The precision of predictions in the added resistance and ship motions is a critical component to the safety, navigations and economic value of shipping in terms of fuel economy. In the past, many predictions of the resistance and ship motions were based on potential theories; however those methods had limitations when dealing with strong nonlinear factors, such as green water on deck and breaking waves.

The current research indicates numerous benefits through the application of rapid developments in computer science and numerical methods. The RANS approach is becoming a powerful method for predicting seakeeping abilities of ships in recent years. It overcomes the shortages of potential theories by taking the water viscosity into consideration and the use of various turbulent models to describe complex flow fields. Many studies have been conducted on RANS for improving the accuracy of computations of the resistance and ship motions. Sato *et al*. (1999) predicted the added resistance and vertical ship motions of Wigley hull and Series 60 in regular head waves by using the marker-density-function method to calculate the nonlinear free surface. Rhee and Stern (2001) performed a validation work on the ship resistance and wave patterns in head waves for modified Wigley hull and their results, support the experimental data well, but the ship form is somewhat simple and the ship motions are restrained. Weymouth (2005) also gave detailed results of the resistance, ship motions, the free surface and the boundary layer of Wigley hull. Chen *et al*. (2002) used a Chimera RANS method to simulate large-amplitude ship roll motions.

Orihara and Miyata (2003) evaluated the added resistance and vertical ship motions of a more complex ship form SR-108 in regular incident waves by applying an overlapping grid system and ship motions were considered. Their computed results of RAOs of heave and pitch motions confirm the experimental data and the degree of agreement is better than the linear methods (the strip theory (Salvesen *et al*., 1970) and the frequency-domain Rankine source method (RSM) (Yoshida *et al*., 2000)). Carrica, Wilson and Stern (2006) presented the numerical results of DTMB 5512 utilizing a single-phase level set method to compute the free surface and a blended model for the turbulent viscosity and the nonlinear. The behaviors of forces and moments are well simulated in the high speed case. In the next year, Carrica *et al*. (2007) broadened the previous efforts and predicted ship motions of DTMB 5512 by means of the single-phase level set method with dynamic overset grids and strong nonlinear responses of ship motions were well predicted.

In 2010, Carrica and Castro, performed self-propulsion computations of KVLCC1, DTMB 5613 and KCS and

Received date: 2012-06-11.
Foundation item: Supported by the National Natural Science Foundation of China (Grant No. 50739004 and 11072154)
***Corresponding author Email:** dcwan@sjtu.edu.cn

dynamic overset grids are used to accomplish the rotation of a propeller. Shen and Wan (2012) provided computational results of the added resistance and ship motions of DTMB 5512 in a wide range of wave steepness by using the solver naoe-FOAM-SJTU. In the case of large wave steepness (ak=0.100), the phenomenon of green water on deck and its influence on the added resistance and ship motions were analyzed numerically.

As mentioned previously, several ship hull forms have already been measured in prior research studies. But most researches of the ITTC S-175 containership on the added resistance and vertical ship motions are based on experiments and strip theories. However, CFD data of S-175 is limited.

The intention of the research is to present computational results of the added resistance and vertical ship motions of the S-175 ship model using RANS, through comparing experimental data and numerical results of the nonlinear strip theory. A wide range of wavelengths ($0.8L_{pp} \le \lambda \le 1.5L_{pp}$) is considered and the computational results will enrich the CFD data of S-175 ship model on added resistance and seakeeping by using RANS method.

All computations are performed by our own in-house unsteady RANS solver naoe-FOAM-SJTU, which is developed based on the open source CFD tool, OpenFOAM. A wave generation and damping module are developed to generate first and high order nonlinear waves, transient extreme waves as well as freak waves (Shen and Wan, 2012, Cao and Wan, 2012). A six-degree-of-freedom (6DoF) motion module coupled with dynamic deformation mesh is also developed to predict ship motions (Shen and Wan, 2011).

2 Numerical methods

2.1 Governing equations

In this paper, the unsteady incompressible viscous flow is addressed using the resolution of RANS:

$$\nabla \cdot \boldsymbol{U} = 0 \tag{1}$$

$$\begin{aligned}\frac{\partial \rho \boldsymbol{U}}{\partial t} + \nabla \cdot (\rho(\boldsymbol{U} - \boldsymbol{U}_g)\boldsymbol{U}) &= -\nabla p_d - \boldsymbol{g} \cdot \boldsymbol{x} \nabla \rho \\ &+ \nabla \cdot (\mu_{eff} \nabla \boldsymbol{U}) + (\nabla \boldsymbol{U}) \cdot \nabla \mu_{eff} + f_\sigma + f_s\end{aligned} \tag{2}$$

where, $\boldsymbol{U}$ is the velocity field; $\boldsymbol{U_g}$ is the velocity of grid nodes; $p_d = p - \rho \boldsymbol{g} \cdot \boldsymbol{x}$ is the dynamic pressure and p is the total pressure; ρ is the mixed density with water and air. $\boldsymbol{g}$ is the gravity acceleration; $\mu_{eff} = \rho(\nu - \nu_t)$ is the effective dynamic viscosity, in which ν and ν_t are kinematic viscosity and eddy viscosity, respectively; ν_t is obtained by applying the SST k-omega turbulence model (Menter, 1994). f_σ is the surface tension due to the free surface between two phases. f_s is the source term introduced due to the sponge layer.

2.2 Interface capturing

The Volume of Fluid (VOF) method with artificial bounded compression techniques is applied to capture the free surface. This method employs volume fraction α to mark different phases (water or air) and it is defined as:

$$\begin{cases}\alpha = 0 & \text{air} \\ \alpha = 1 & \text{water} \\ 0 < \alpha < 1 & \text{interface}\end{cases} \tag{3}$$

The value of α in each cell indicates that in which kind of fluid the cell is and α obeys a transport equation as below:

$$\frac{\partial \alpha}{\partial t} + \nabla \cdot \left[(\boldsymbol{U} - \boldsymbol{U}_g)\alpha \right] + \nabla \cdot \left[\boldsymbol{U}_r (1 - \alpha)\alpha \right] = 0 \tag{4}$$

in which, $\boldsymbol{U}_r$ is a velocity field compressing the interface and expressed as:

$$\boldsymbol{U}_{r,f} = \boldsymbol{n}_f \min\left\{ C_\alpha \frac{|\phi|}{|\boldsymbol{S}_f|}, \max\left(\frac{|\phi|}{|\boldsymbol{S}_f|} \right) \right\} \tag{5}$$

in which, C_α is a compression coefficient controlling the degree of compression. The larger C_α is, the more significant the compression is and it is set as 1.0 in current work. ϕ is face volume flux and the flux of grid velocities is included due to the implement of dynamic deformation mesh. $\mathbf{S}_f$ is the normal vector of a cell face and its norm equals to the area of the cell face. $\boldsymbol{n}_f$ is the unit normal vector of the interface and expressed as:

$$\boldsymbol{n}_f = \frac{(\nabla \alpha)_f}{\left| (\nabla \alpha)_f + \delta \right|} \tag{6}$$

in which, δ is a very small number used as a stable factor.

After the capture of interface, the surface tension term in Eq.(2) can be calculated as:

$$f_\sigma = \sigma \kappa \nabla \alpha \tag{7}$$

in which, σ is the surface tension coefficient and equals to 0.07kg/s^2 in present work. κ is the curvature of the interface, given by:

$$\kappa = -\nabla \cdot \left(\frac{\nabla \alpha}{|\nabla \alpha|} \right) \tag{8}$$

2.3 Dynamic deformation mesh

Dynamic deformation mesh is applied to predict the ship motions by moving grid nodes together with the ship hull. The position of each grid node is resolved by the Laplace equation below:

$$\nabla \cdot (\gamma \nabla \boldsymbol{x}_g) = 0 \tag{9}$$

in which, $\boldsymbol{x}_g$ is the displacement of a grid node and γ is the diffusivity coefficient defined as:

$$\gamma = \frac{1}{r^2} \tag{10}$$

in which, r is the distance between the cell center and the moving boundary (the ship hull in present work).

2.4 Wave generation

In the wave generation module, the inlet boundary conditions

of α in the VOF transport Eq.(4) and $\boldsymbol{U}(u,v,w)$ in RANS a Eq.(1) and Eq.(2) are set to generate head waves in the research as follows:

$$\zeta(x,t) = a\cos(kx - \omega_e t) \tag{11}$$

$$u(x,y,z,t) = U_0 + a\omega e^{kz}\cos(kx - \omega_e t) \tag{12}$$

$$w(x,y,z,t) = a\omega e^{kz}\sin(kx - \omega_e t) \tag{13}$$

in which, ζ is transient wave elevation; a, ω and k are wave amplitude, wave frequency and wave number, respectively; U_0 is ship speed; $\omega_e = \omega + kU_0$ is encounter frequency in head waves. At t=0, the crest of a wave reaches the bow of ship model at the position of x=0.

2.5 Sponge layer

A sponge layer is setup at the outlet of the computational domain to avoid wave reflection from the outlet boundary. The term of f_s is introduced into Eq.(2) for absorption of waves and defined as:

$$f_s(x) = \begin{cases} -\rho\alpha_s\left(\dfrac{x - x_s}{L_s}\right)^2(\boldsymbol{U} - \boldsymbol{U}_{\text{ref}}) & \text{in the sponge layer} \\ 0 & \text{out of the sponge layer} \end{cases} \tag{14}$$

in which, ρ is the water density. The α_s is an artificial viscosity coefficient controlling the intensity of the sponge layer and set as 20 in current research. The x_s is the coordinate of the start position of the sponge layer and L_s is the length of the sponge layer. $\boldsymbol{U}_{\text{ref}}$ is a reference velocity and is equal to velocity at the inlet boundary. It will result in equal velocities at the inlet and outlet boundaries and guarantee the mass conversation of the entire computational domain. The source term f_s have no effects on the domain out of the sponge layer.

2.6 6DOF motions

When a ship is advancing in regular head waves, the accurate prediction of ship motions is important because of the influences on the calculations of added resistance. Currently, a 6DoF module has been developed and implemented to predict accurately the ship motions. The study utilized two coordinate systems for solving the 6DoF equations.

One coordinate system is earth fixed and the other is body fixed. The detailed description of body-fixed system and the calculation of force, moment, acceleration, velocity and global displacement of grid nodes can be found in (Shen and Wan, 2012).

3 Ship geometry and case conditions

The ITTC S-175 containership with a scale of 1:40 is employed for the numerical calculations. The S-175 containership is a standard ship used by ITTC (ITTC, 1978, ITTC, 1981) as a benchmark hull form to study sea-keeping capability and several institutions have tested on this hull form. Fig. 1 presents the body lines. The main particulars of the ship model used in the current research are provided in Table 1. The findings are the same as the model, used in the tests conducted at the Laboratory of Ship Dynamics of the EI Pardo Model Basin in Madrid (Fonseca and Guedes, 2004).

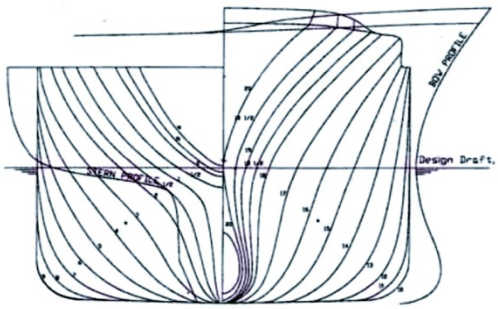

Fig. 1 S-175 containership body lines

Table 1 S-175 main particulars

Particular /Unit	Symbol	Model
Length between perpendiculars/m	L_{pp}	4.4
Breadth/m	B	0.64
Depth/m	D	0.39
Draught/m	T	0.24
Displacement/kg	Δ	370.94
Block coefficient	C_b	0.572
Pitch radius of gyration	K_{yy}/L_{pp}	0.24

The body-fixed coordinate system is defined, with respect to the mean position of the model illustrated in Fig. 2.

Fig. 2 Body-fixed coordinate system

Presently, four wave conditions covering a wide range of wavelengths are regarded in the research. The detailed information of the wave conditions is presented in Table 2. λ is the wave length, ak is the wave steepness and T_e is the encounter period.

Table 2 Wave conditions

L_{pp}/λ	λ /m	ak	T_e /s
0.657	6.697	0.05	1.373
0.881	4.992	0.05	1.126
1.122	3.922	0.05	0.953
1.260	3.493	0.05	0.878

In all cases, the ship speed is 1.6425 m/s with Fn=0.25 and all the incident waves are regular head waves. Only heave and

pitch motions are considered in the current research, because they are the most severe motions in the head waves and have the greater influence on the added resistance than any other ship motions.

4 Computation domain

The unstructured mesh used in present work is generated by snappyHexMesh, provided by OpenFOAM. The detail of the mesh is illustrated in Fig.3. The calculation domain is $-1.0L_{pp} < x < 3.0L_{pp}, 0 < y < 1.0L_{pp}, -1.0L_{pp} < z < 1.0L_{pp}$.

The total number of cells is around 1.4 million. It should be noted that only half of the ship hull is used in the calculations, thus a 'symmetry' boundary condition can be modified at the center plane boundary to optimize the calculations.

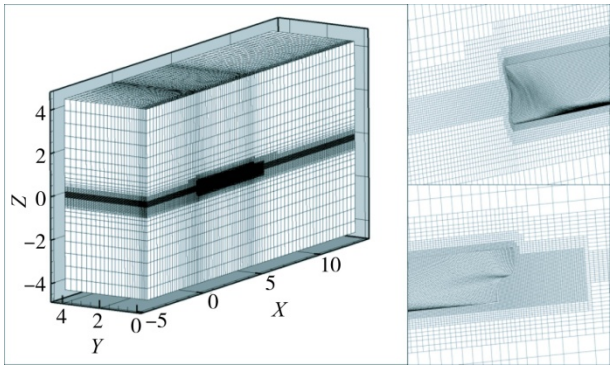

Fig. 3 Mesh used for numerical computations

5 Discussion of results

5.1 Added resistance

The added resistance is measured as the difference between the mean resistance in waves and the resistance in calm water at the same speed. The results of the added resistance are presented in a nondimensional form by the following equation:

$$C_{aw} = \frac{R_{aw}}{\rho g a^2 B^2 / L_{pp}} \tag{15}$$

in which, C_{aw} is the nondimensional added resistance, also called added resistance coefficient. R_{aw} is the added resistance. ρ is the density of water. g is the acceleration of gravity. a is the wave amplitude. B and L_{pp} are presented in Table1. Fujii and Takahashi (1975) have used a 1:50 model of this ship to measure the added resistance in regular waves with different wave directions. The comparison amongst current research, the Fujii report and the strip theory is provided in Fig.4. The results of the strip theory are taken from the report of Journée (2001) using both the radiated energy method of Gerritsma and Beukelman (1972) and the integrated pressure method of Boese (1970). In Fig.4, circles and triangles represent the results of the experimental findings, respectively. The continuous lines and dashed lines represent results of the strip theory.

Except for the case $L_{pp}/\lambda = 1.122$, the numerical results of current work are better than those of the strip theory, especially in the short wave length case ($L_{pp}/\lambda = 1.260$). When the wave length is around the ship length, the added resistance reaches its peak value. The added resistance is overestimated in this range of wave length by the strip theory and the results of the RANS simulation are better in the same case by comparison.

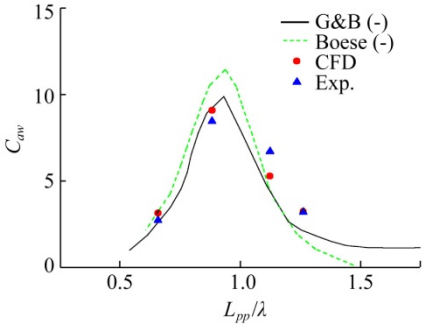

Fig. 4 Comparison of added resistance

5.2 Heave and pitch motions

The comparisons among the CFD simulations, experiments and the nonlinear strip theory are presented in this section and illustrated in Fig.5 and Fig.6. The experimental results are given in (Fonseca and Guedes, 2004).

Experimental conditions involve different wave lengths and height. Unfortunately, the wave condition is H_w/L_w=1/63 in current study and the closest wave condition in the experiments is H_w/L_w =1/60. But these two wave conditions are very similar and considering the fact that the H_w/L_w has little influence on the transfer functions of the vertical motions in these wave conditions, it is reasonable to make a comparison of them. In addition, Fonseca and Soares (2005) presented the comparison between the experimental data and their numerical results by the nonlinear strip theory with wave conditions of H_w/L_w =1/120, H_w/L_w =1/80 and H_w/L_w =1/40 in their paper. The results of transfer functions in the experiments indicate the same fact that the value of H_w/L_w has little influence on the transfer functions of both vertical ship motions when H_w/L_w is not very large. Based on this fact, the results of both experiments and the nonlinear strip theory in the case H_w/L_w =1/80 are also given in the figures for comparison.

The responses of heave and pitch motions are respectively presented in Fig.5 and Fig.6 in the form of transfer functions. The transfer functions of heave and pitch motions are defined as:

$$TF_3 = \frac{x_{3_1}}{a} \tag{16}$$

$$TF_5 = \frac{x_{5_1}}{ak} \tag{17}$$

in which, TF_3 and TF_5 are the transfer functions of heave

and pitch motions, respectively. x_{3_1} and x_{5_1} are the 1st Fourier Series (FS) harmonic amplitudes (Carrica *et al*., 2006) of heave and pitch motions respectively.

In Fig.5 and Fig.6, the line with hollow squares and the triangle symbols represent the experimental data. The solid square symbols represent the result of CFD predictions in current work and the dash line represents the results of the nonlinear strip theory. In each figure, results in the same wave condition are presented in the same color for comparison's sake. Moreover, the CFD results at H_w/L_w =1/63 are presented as the same color as the experimental data at H_w/L_w =1/60.

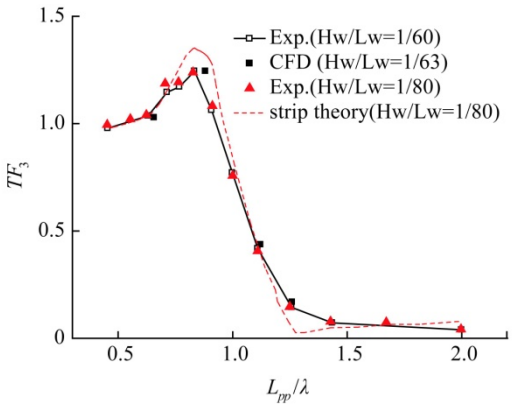

Fig.5 Transfer function of heave as a function of the wave frequency

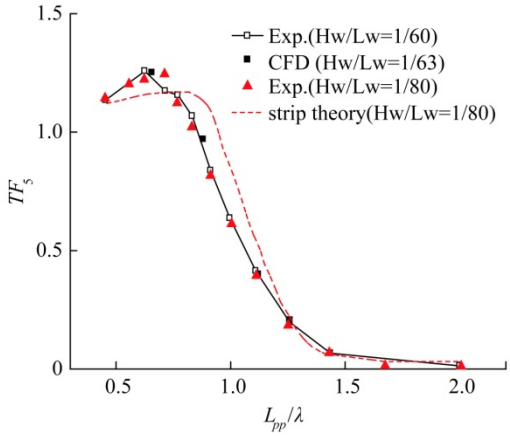

Fig. 6 Transfer function of pitch as a function of the wave frequency

The results from both figures indicate, the experimental results of transfer functions are very similar in the wave conditions of H_w/L_w =1/60 and H_w/L_w =1/80 for both vertical ship motions. The findings have once again proven the rationality for comparisons between the CFD results at H_w/L_w =1/63 and the experimental results at H_w/L_w =1/60.

The curves of transfer functions of both vertical ship motions have peak values and the corresponding wavelength of the peak place of the heave motion is larger and closer to the ship length than that of the peak place of the pitch motion. After the peak places, and transfer functions decrease sharply to almost zero there is a decrease of the wave length.

From Fig.5 and Fig.6, we can conclude that the results of RANS simulations on vertical ship motions had better results than the nonlinear strip theory, especially as the wavelength is close to the ship length, which means the wave frequency is close to the resonance frequency. In this range of wavelengths vertical ship motions have relatively large amplitude and are strongly influenced by nonlinear factors, *i.e.* wave breaking. The numerical results of the nonlinear strip theory when the wavelength is close to the ship length are fair worse than results in other ranges of wavelengths. In comparison, the RANS simulations can predict the value of both vertical ship motions more accurately than the nonlinear strip theory in a wide range of wavelengths, especially around the peak place.

2nd harmonic amplitudes of heave and pitch motions are presented in Fig.7 and Fig.8. x_{3_2} and x_{5_2} are the 2nd Fourier Series (FS) harmonic amplitudes of heave and pitch motions respectively. The results of heave and pitch motions are nondimensionalised by the wave amplitude (a) and the wave steepness (ak), respectively.

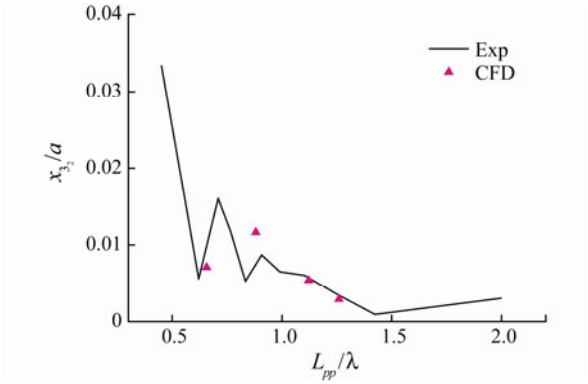

Fig. 7 Second-order harmonic amplitude of the nondimensional heave motion

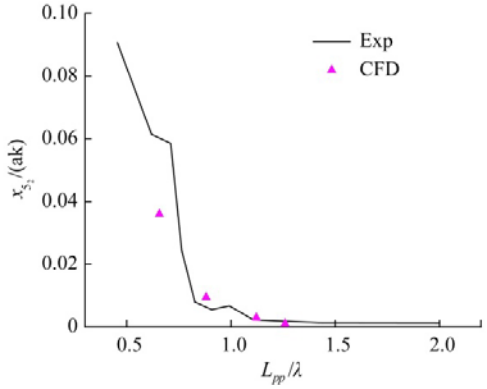

Fig. 8 Second-order harmonic amplitude of the nondimensional pitch motion

The 2nd harmonic amplitudes are the main components of the nonlinearity of vertical motion responses and calculations using the nonlinear strip theory are hard to handle these nonlinear motion components. In comparison with the 1st harmonic amplitudes, the higher order effects are relatively small for the vertical motions, and the changing trends are quite obvious. The 2nd harmonic amplitudes of both vertical ship motions increased rapidly with the increase of the wavelength around the resonance frequency. The results are consistent with the descriptions in (Fonseca and Soares, 2004).

In Fig.7 and Fig.8, RANS simulations predict the 2nd harmonic amplitudes well, especially when $L_{pp}/\lambda \geq 1.0$. The results when $L_{pp}/\lambda < 1.0$ still need to be improved in the further research.

5.3 Free surface

In this section, simulating results of the free surface in the typical case ($L_{pp}/\lambda = 0.881$) is presented briefly. The discussions above show that the added resistance is the largest and vertical ship motions are the most severe in the case of $L_{pp}/\lambda = 0.881$. Free surface at four instants over an encounter period is illustrated in Fig. 9.

At t/T=0.00, the crest arrives at the bow and the trim angle reaches its negative peak. At this instant, the breaking wave is the most notable in an encounter period and its height is already above the freeboard. During the next half of the encounter period, the hull is trimming by stern and the trim angle reaches its positive peak at t/T=0.50. Then, the hull starts to trim by bow.

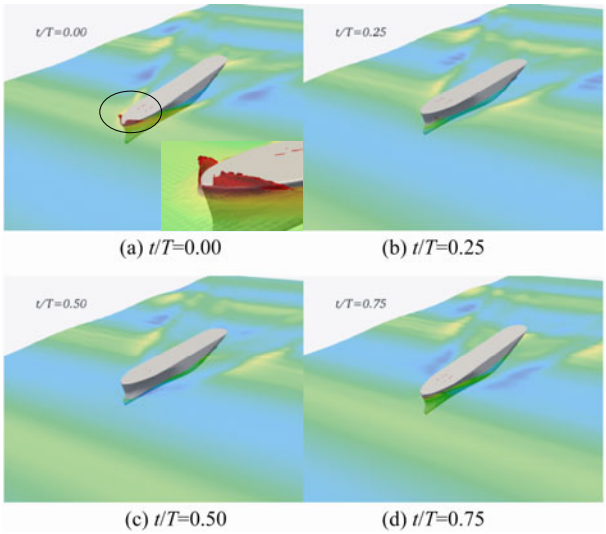

Fig. 9 Free surface at four instants over an encounter period at $L_{pp}/\lambda = 0.881$

The simulations of the free surface provided evidence that the presented naoe-FOAM-SJTU solver has the ability to simulate strongly nonlinear phenomena of wave breaking.

6 Conclusions

The RANS numerical simulation of the added resistance and vertical ship motions of the ITTC S-175 containership in head waves with wide range of wavelengths by our own in-house solver naoe-FOAM-SJTU is presented. The comparison between numerical results, experimental data and nonlinear strip theory results were quantified. The analysis of added resistance shows the accuracy of the simulations is higher than the nonlinear theory. The study confirms there are more advantages of utilizing the naoe-FOAM-SJTU solver for improving the prediction of vertical ship motions. The results of transfer functions for the vertical ship motions are in line with the experimental data, especially concerning the resonance frequency.

The test results indicate the presented naoe-FOAM-SJTU solver is more powerful for handling large-amplitude ship motions with strong nonlinear factors. The 2nd harmonic amplitudes, which are the main components of the nonlinear responses of ship motions, were also examined in the research paper. Although the study briefly touched on the issue, the findings indicate the presented solver can still predict well and the tendencies of the values with wavelength changes were illustrated clearly. In the final section of the research paper, the simulation results of free surface were specified and the phenomenon of wave breaking was clearly simulated. Future research will include precision of the solver calculations improvements, especially in the cases of larger wave steepness and the nonlinearity of responses of resistance and ship motions.

Acknowledgement

This work is supported by the National Natural Science Foundation of China (Grant No. 50739004 and 11072154), Foundation of State Key Laboratory of Ocean Engineering of China (GKZD 010053-11), the Program for Professor of Special Appointment (Eastern Scholar) at Shanghai Institutions of Higher Learning(2008007), and The Lloyd's Register Educational Trust (The LRET) through the joint canter involving University College London, Shanghai Jiao Tong University and Harbin Engineering University, to which the authors are most grateful.

References

Boese P (1970). Eine Einfache Methode zur Berechnung der Wiederstandserhöhung eines Schiffes in Seegang. Institut für Schiffbau der Universität Hamburg, Bericht, 258.

Cao HJ, Zha JJ (2011). Numerical simulation of wave run-up around a vertical cylinder. *Proceedings of the Twenty-first (2011) International Offshore and Polar Engineering Conference*, Maui, Hawaii, USA.

Cao HJ, Wan DC (2012). Numerical investigation of extreme wave effects on cylindrical offshore structures. *Proceedings of the*

Twenty-second International Offshore and Polar Engineering Conference (ISOPE), Rhodes, Greece.

Carrica PM, Wilson RV (2006). Unsteady RANS simulation of the ship forward speed diffraction problem. *Computers & Fluids*, **35**(6), 545-570.

Carrica PM, Wilson RV (2007). Ship motions using single-phase level set with dynamic overset grids. *Computers & Fluids*, **36**(9), 1415-1433.

Carrica PM, Castro AM (2010). Self-propulsion computations using a speed controller and a discretized propeller with dynamic overset grids. *Journal of Marine Science and Technology*, **15**(4), 316-330.

Chen HC, Liu T (2002). Time-domain Simulation of large-amplitude ship roll motions by a Chimera RANS method. *International Journal of Offshore and Polar Engineering*, **12**(3), 206-212.

Fonseca N, Soares CG (2004). Experimental investigation of the nonlinear effects on the vertical motions and loads of a containership in regular waves. *Journal of Ship Research*, **48**(2), 118-147.

Fonseca N, Soares CG (2005). Comparison between experimental and numerical results of the nonlinear vertical ship motions and loads on a containership in regular waves. *International Shipbuilding Progress*, **52**(1), 57-89.

Fujii H, Takahashi T (1975). Experimental study on the resistance increase of a ship in regular oblique waves. *Proc. of 14th ITTC*, **4**, 351-360.

Gerritsma J. Beukelman W (1972). Analysis of the resistance increase in waves of a fast cargo ship. *International Shipbuilding Progress*, **19**, 217.

ITTC (1978). 15th ITTC Seakeeping Committee Report. *Proceeding of the 15th ITTC*, The Hague.

ITTC (1981). 16th ITTC Seakeeping Committee Report. *Proceeding of the 16th ITTC*, Leningrad.

Journée J (2001). Verification and validation of ship motions program SEAWAY. Delft University of Technology Shiphydromechanics Laboratory, Report1213a.

Menter FR (1994). Two-equation eddy-viscosity turbulence models for engineering applications. *AIAA Journal*, **32**(8), 1598-1605.

Orihara H, Miyata H (2003). Evaluation of added resistance in regular incident waves by computational fluid dynamics motion simulation using an overlapping grid system. *Journal of Marine Science and Technology*, **8**(2), 47-60.

Rhee SH, Stern F (2001). Unsteady RANS method for surface ship boundary layer and wake and wave field. *International Journal for Numerical Methods in Fluids*, **37**(4), 445-478.

Salvesen, N., E. Tuck (1970). Ship motions and sea loads. *Trans. SNAME*, **78**, 250-287.

Sato Y, Miyata H (1999). CFD simulation of 3-dimensional motion of a ship in waves: Application to an advancing ship in regular heading waves. *Journal of Marine Science and Technology*, **4**(3), 108-116.

Shen ZR, Jiang L (2011). RANS simulations of benchmark ships based on open source code. *Proceedings of the Seventh International Workshop on Ship Hydrodynamics (IWSH'2011)*, Shanghai, China.

Shen ZR, Wan DC (2012). RANS computations of added resistance and motions of ship in head waves. *Proceedings of Twenty-second(2012) Ocean(Offshore) and Polar Engineering Conference*, Rhodes, Greece, ISOPE.

Weymouth GD, Wilson RV (2005). Rans computational fluid dynamics predictions of pitch and heave ship motions in head seas. *Journal of Ship Research*, **49**(2), 80-97.

Yoshida H, Miyake S (2000). Prediction of seakeeping performance of a ship by rankine source method (Part. 1)-Improvement on the Free Surface Panel Resolution near the Ship. *Journal-Kansai Society of Naval Architects Japan*, 167-172.

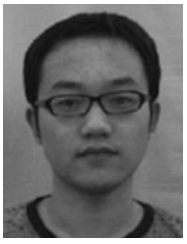

Haixuan Ye is a graduate student in School of Naval Architecture, Ocean and Civil Engineering, Shanghai Jiao Tong University. His current research field includes computational simulations of the added resistance, force and motion responses of ships when advancing in seaways.

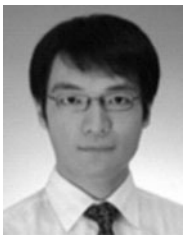

Zhirong Shen is currently a PhD candidate in School of Naval Architecture, Ocean and Civil Engineering, Shanghai Jiao Tong University. His research interests include computational ship hydrodynamics, wave generation method and a 6DoF motion of ship based on OpenFOAM. He is now working on the implementation of overset grid technique into OpenFOAM.

Decheng Wan is a professor of School of Naval Architecture, Ocean and Civil Engineering, Shanghai Jiao Tong University, and a distinguished professor of Shanghai Eastern Scholar. His research interests include marine hydrodynamics and computational fluid dynamics, marine numerical wave tank, nonlinear wave theory, fluid-structure interaction, high performance computation on complex flows, *etc*.